Improving Speed Characteristics of High Torque Density Motors for Physical Human-Robot Interaction using Independent 3-Phase Winding Structure

Junghwan Park and Handdeut Chang *

Posted Date: 29 March 2024

doi: 10.20944/preprints202403.1881.v1

Keywords: High Torque Density Motor; Safe pHRI(physical Human-Robot interaction); Independent 3-phase; Motor Controller

Article

Improving Speed Characteristics of High Torque Density Motors for Physical Human-Robot Interaction using Independent 3-Phase Winding Structure

Junghwan Park and Handdeut Chang *

Department of Mechanical Engineering, Incheon National University, 119, Academy-ro, Yeonsu-gu, Incheon 22012, Republic of Korea; park_hault@inu.ac.kr

* Correspondence: onemeanl@inu.ac.kr

Abstract: Recently, due to the decrease in labor force, increase in labor costs, and the desire for improved quality of life, research on robots has been actively conducted to address these issues. However, it is currently difficult to find robots that physically interact with humans. The reason is that the actuators of robots do not have high torque density on their own. To solve this problem, high torque density motors, such as proprioceptive actuators, are being researched. However, the torque density is still insufficient for physical interaction with humans, so we have developed a motor with higher torque density. However, high torque density motors have the disadvantage of lower speed characteristics due to increased Back-EMF. Therefore, to address the deterioration of speed characteristics in the developed motor, we applied the Independent 3-Phase winding structure to improve the speed characteristics. Consequently, through comparison with Y-Connection and Delta-Connection, we propose the most suitable winding structure for high torque density motors intended for physical interaction with humans.

Keywords: high torque density motor; safe phri(physical human-robot interaction); independent 3-phase; motor controller

1. Introduction

As the workforce declines, labor costs rise, and the desire for improved living standards grows, the study of robotics across various domains has experienced a notable increase to address these societal challenges and demands. However, in modern environments where humans are closely involved with pHRI(physical Human-Robot Interaction), the prevalent robots are mostly guided robots and robotic vacuum cleaners. It's challenging to find robots that physically interact with humans. The main issue stems from the insufficient torque density produced by the robot's propulsion systems, resulting in the inevitable need for reducers in the joints of robots. As a result, this decreasing in joint back-drivability poses a significant risk to humans in unexpected collisions [1]. This is the primary reason why robots currently have a limited presence around humans.

The main methods currently used for robotic actuators are hydraulic, pneumatic, and motor-based systems, each with its own advantages and disadvantages. Hydraulic systems have the advantage of excellent torque generation capabilities, but they suffer from hydraulic fluid leakage, require additional equipment such as pumps leading to increased maintenance, noise, and significant weight [2]. Pneumatic systems are clean and easy to maintain, but like hydraulic systems, they require additional equipment and are sensitive to small changes in pressure or flow rate, making them difficult to control [3]. As a result, hydraulic and pneumatic actuators present many challenges when used in robots that operate in close proximity to humans. On the other hand, electric motors offer relatively low cost, cleanliness, small noise, and volume, making them suitable for robotic joints that physically interact with humans in their vicinity. However, the torque density of conventional BLDC motors is insufficient for robots to achieve specific objectives, necessitating the inevitable use of

 doi:10.20944/preprints202403.1881.v1

reducers with high gear ratios. Additionally, the nonlinear friction generated in the gears makes it difficult to estimate torque from the motor current, making the use of torque sensors essential.

Therefore, to address these issues, an actuator called a proprioceptive actuator was developed [4–8]. Proprioceptive actuators do not require a torque sensor and use a high torque density motor with a low gear ratio transmission and a current sensor in the current controller as a proprioceptive sensor. However, the torque density is still low, and the pulsating torque, which can be amplified by the gear reducer, is high. Inspired by the concept of proprioceptive actuators, we developed a high torque density motor to implement in legged or wearable robots for physical interactions.

However, high torque density motors also have high back-EMF, which results in lower speed characteristics. Therefore, this paper aims to solve the problem of reduced speed characteristics in high torque density motors by applying the Independent 3-Phase winding structure method. Unlike conventional Y-Connection and Delta-Connection winding structures, the Independent 3-Phase BLDC Motor allows the full voltage to be applied to a single phase without voltage division from the voltage source [9]. This enables the use of a higher phase voltage, which can improve low-speed characteristics. Accordingly, this paper verifies the effectiveness of the Independent 3-Phase BLDC Motor through comparative experiments of speed characteristics. The experiments compare the conventional Y-Connection winding structure, Delta-Connection winding structure, and the proposed Independent 3-Phase winding structure.

2. 3-Phase BLDC Motor and Controller Design

We developed a motor optimized for high torque density, as shown in Figure 1, by applying various design elements such as strong magnets, minimized air gap between the stator and rotor, and a Halbach array to prevent flux leakage and concentrate flux on the stator. The mass distribution of the developed motor is presented in Table 1, and its characteristic parameters are listed in Table 2. we conduct experiments based on this developed motor with different winding structures.

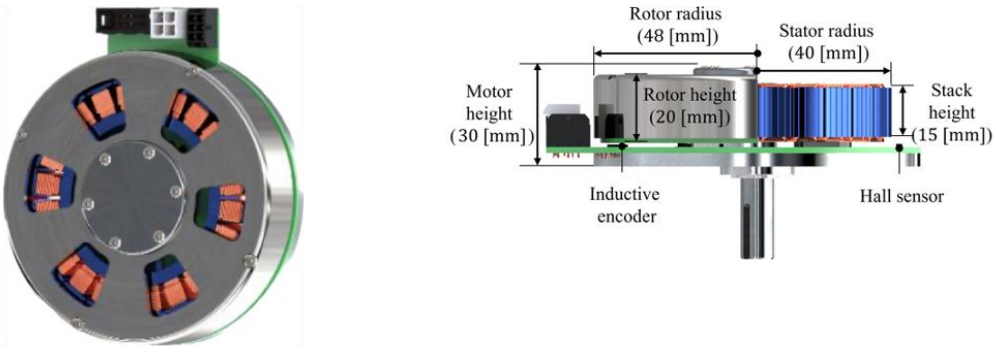

(**a**) (**b**)

Figure 1. (**a**) Developed Motor's front view; (**b**) Developed Motor's side view.

Table 1. Mass Distribution of the Developed Motor.

Parameters of motors	Rotor (magnet and yoke)	Rotor (housing and axis)	Stator	Stator housing	Bearing and PCB	Total mass (frameless)	Total mass (housed)
Unit [g]	150	80	280	55	30	430	595

Table 2. Developed Motor Characteristic Parameters (Y-Connection Winding Structure).

Parameters motors	Torque const. [Nm/A]	Phase resistance [Ω]	Motor const. [Nm/$\sqrt{W}$]	Nominal Torque [Nm]	Cogging Torque [Nm]	Continuous Torque Density [Nm/kg]

 doi:10.20944/preprints202403.1881.v1

Developed Motor	0.755	0.717	0.630	3.45	0.021	8.03

2.1. 3-Phase BLDC motor Governing Equations

The governing equations for the characteristics of Y-Connection, Delta-Connection, and Independent 3-Phase Motors are all the same, making it easy to compare the characteristics of each winding method using the following equations. The voltage equation is expressed as Equation (1), the output power as Equation (2), and the torque equation as Equation (3) [14,15].

$$V_n = R_s I_n + L_s \frac{I_n}{dt} + E_n \tag{1}$$

$$P_e = E_a I_a + E_b I_b + E_c I_c \tag{2}$$

$$T_e = \frac{P_e}{W_m} = \frac{E_a I_a + E_b I_b + E_c I_c}{W_m} \tag{3}$$

Here, V_n $(n = a, b, c \text{ or } ab, bc, ca)$ represents either the phase voltage or line voltage depending on the winding method of the stator, R_s signifies the resistance of the stator, L_s denotes the inductance of the stator, I_n $(n = a, b, c)$ represents the phase current flowing through each of the three phases, E_n $(n = a, b, c,)$ signifies the back electromotive force generated in each phase, and W_m represents the mechanical angular velocity of the rotor.

$$V = K_t \omega \tag{4}$$

$$E_a = Vsin(\omega t)\ , \qquad E_b = Vsin\left(\omega t + \frac{2\pi}{3}\right)\ , \quad E_c = Vsin\left(\omega t - \frac{2\pi}{3}\right) \tag{5}$$

Here, ω represents the angular frequency, The Back EMF for each phase is represented by Equation (5), with each phase having a phase difference of $\frac{2\pi}{3}$.

2.2. 3-Phase BLDC Motors Winding Structure

For BLDC motors, different characteristics can be achieved depending on the winding structure of the stator. The Y-Connection is preferred for applications requiring high torque and low speed due to its simple structure and relatively high efficiency. On the other hand, the Delta-Connection is suitable for applications with low torque and high speed as it can reduce the phase impedance and widen the operating range. Especially in independent power supply drive systems powered by low-voltage batteries, the Delta-Connection is frequently used [12,13]. In contrast to the two commonly used connection methods, the approach we propose utilizes an independent 3-Phase method, known as the single-phase excitation structure, where voltage is applied independently to each winding without contact points between them.

In the case of the Independent 3-Phase system's wiring structure, there is almost no increase in the size and weight of the motor itself. Unlike the Y-Connection or Delta-Connection methods, where one voltage source is split into two or three phases, in the Independent 3-Phase system, one voltage source is allocated to each phase. This results in an increase in phase voltage. This increase in phase voltage implies an increase in phase current when resistance and inductance are constant. Therefore, this increase in phase current translates into an increase in the torque that the motor can exert at the same voltage, thereby enhancing the torque density of the motor. Since the control method is generally similar to that of commonly used wiring methods, changing only the winding method presents no significant challenge, enabling the motor to achieve higher torque density. This paper validates the efficacy of the Independent 3-Phase BLDC Motor through comparative experiments with Y-Connection BLDC motors and Delta-Connection BLDC motors.

 doi:10.20944/preprints202403.1881.v1

2.2.1. Y-Connection BLDC Motor Design

In the case of a Y-Connection BLDC motor, each of the three phases forms a neutral point, as shown in Figure 1 (a). The excitation structure applied to the armature is a 2-phase excitation system, as depicted in Figure 1 (b), where two phases are excited by one voltage source. In this system, since two phases are excited by one voltage source, the available voltage per phase is reduced by half [16]. The reason why Y-connected BLDC motors are more commonly used than Delta-connected BLDC motors is that by not grounding the neutral point, they can remove the zero-sequence component of the third harmonic that causes inductive interference, thereby improving the waveform and reducing the effect of ripple on the BLDC motor operation. Additionally, the relationship between line-to-line voltage and phase voltage is advantageous for high voltages, and corona discharge and deterioration are prevented.

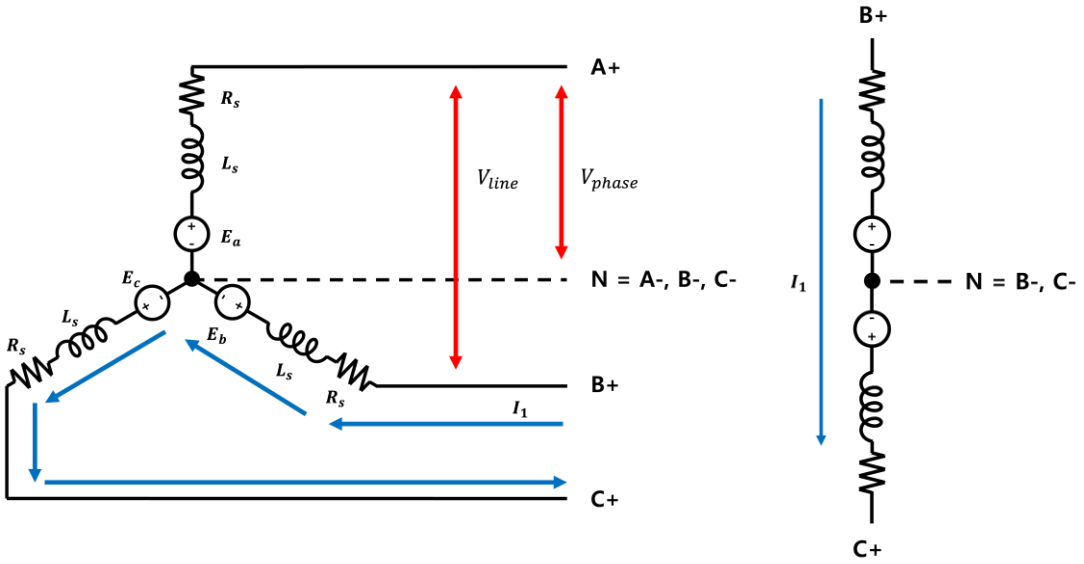

Figure 1. (a) Equivalent Circuit of Y-Connection BLDC Motor (b) Excitation System of Y-Connection BLDC Motor (2-Phase Excitation).

$$V_{line} = \sqrt{3}V_{phase}\,,\quad I_{line} = I_{phase} \tag{7}$$

$$|E_b - E_c| = V\left|sin\left(\omega t + \frac{2\pi}{3}\right) - sin\left(\omega t - \frac{2\pi}{3}\right)\right| \tag{8}$$

$$= V\left|2cos\omega sin\frac{2\pi}{3}\right| \tag{9}$$

$$= \sqrt{3}k_t\omega|cos\omega t| \tag{10}$$

Here, V_{line} represents the line-to-line voltage, V_{phase} represents the phase voltage, I_{line} represents the line current, I_{phase} represents the phase current and k_t denotes the Back EMF constant. In the case of Y-Connection, the line-to-line voltage is $\sqrt{3}$ times greater than the phase voltage. The motor reaches saturation speed at ω where Equation (10) is satisfied [17].

2.2.2. Delta-Connection BLDC Motor Design

In the case of Delta-Connection BLDC motors, one end of each winding is connected to the neighboring end of the adjacent winding, creating a total of 3 winding junctions, as shown in Figure 2 (a). When voltage is applied to the stator, as illustrated in Figure 2 (b), it forms a 3-Phase excitation

Preprints.org (www.preprints.org) | NOT PEER-REVIEWED | Posted: 29 March 2024 doi:10.20944/preprints202403.1881.v1

system where all three phases are energized by a single voltage source [16]. With this system, since all three phases are excited by a single voltage source. The uneven distribution of voltage applied to each phase, as seen in Figure 2 (b), creates ripples in the operation of the BLDC motor [18].

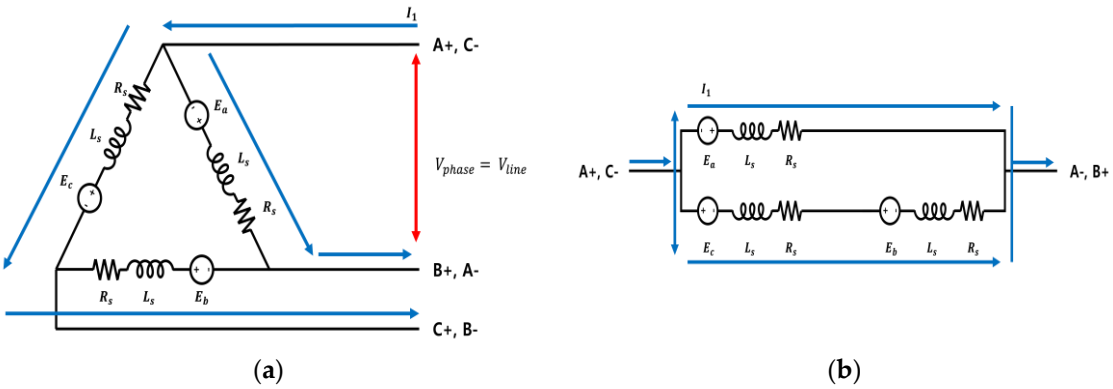

(**a**) (**b**)

Figure 2. (a) Equivalent Circuit of Delta-Connection BLDC Motor (b) Excitation System of Delta-Connection BLDC Motor (3-Phase Excitation).

$$V_{line} = V_{phase}, \quad I_{line} = \sqrt{3} I_{phase} \tag{11}$$

$$|E_b + E_c| = V \left| sin\left(\omega t + \frac{2\pi}{3}\right) + sin\left(\omega t - \frac{2\pi}{3}\right) \right| \tag{12}$$

$$= V \left| 2 sin\omega t cos\frac{2\pi}{3} \right| \tag{13}$$

$$= k_t \omega |sin\omega t| \tag{14}$$

$$|E_a| = k_t \omega |sin\omega t| \tag{15}$$

In the case of Delta-Connection, the line-to-line voltage is equal to the phase voltage, while the line current is $\sqrt{3}$ times greater than the phase voltage. The motor reaches saturation speed at ω where Equations (14) and (15) are satisfied and compared to Equation (10) for Y-Connection BLDC Motor, it has a saturation point that is $\sqrt{3}$ times higher [17].

2.2.3. Independent 3-Phase BLDC Motor Design

In the Independent 3-Phase BLDC Motor, unlike Y-Connection and Delta-Connection methods, each phase is separate and distinct without any junction points, as illustrated in Figure 3 (a) Additionally, the electrical location of each phase in the motor's structure is identical to that of the Y-Connection and Delta-Connection methods. This adds no complexity to motor control and facilitates easy handling. In the Independent 3-Phase BLDC Motor, unlike the previous methods, when voltage is applied to one phase, it is exclusively applied to that phase. The voltage is not distributed among the other phases. The increase in applied voltage signifies an increase in phase current when the resistance and inductance of the stator remain constant, as indicated by Equation (3), leading to an increase in torque [13].

Preprints.org (www.preprints.org) | NOT PEER-REVIEWED | Posted: 29 March 2024 doi:10.20944/preprints202403.1881.v1

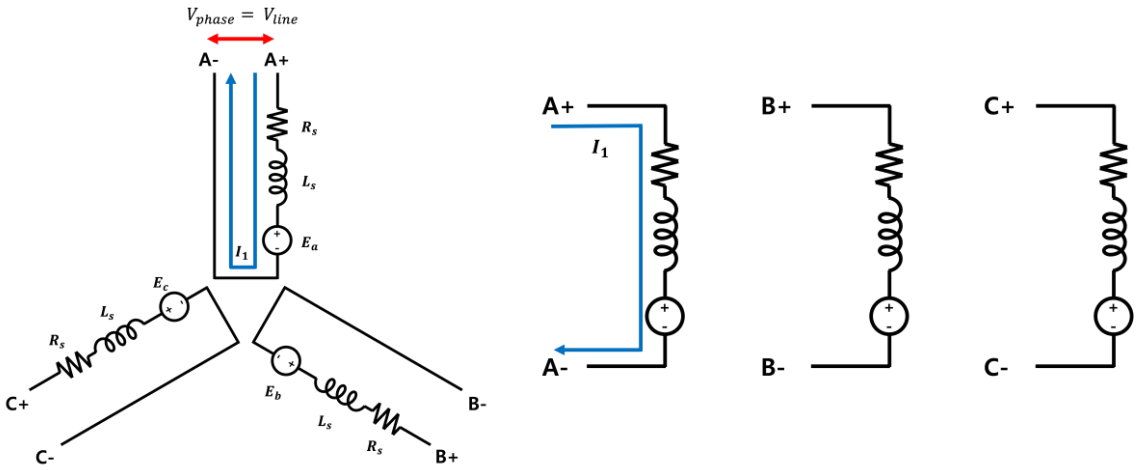

Figure 3. (a) Equivalent Circuit of Independent 3-Phase BLDC Motor (b) Excitation System of Independent 3-Phase BLDC Motor (Single-Phase Excitation).

$$|E_a| = k_t\omega|sin\omega t| \tag{16}$$

$$|E_b| = k_t\omega\left|\sin\left(\omega t + \frac{2\pi}{3}\right)\right| \tag{17}$$

$$|E_c| = k_t\omega\left|sin\left(\omega t - \frac{2\pi}{3}\right)\right| \tag{18}$$

In the case of the Independent 3-Phase BLDC Motor, unlike the Y-Connection BLDC Motor and Delta-Connection BLDC Motor, there is no difference in the magnitudes of line voltage and phase voltage as well as line current and phase current. The speed of the BLDC Motor saturates at ω, which satisfies Equation (16).

2.3. 3-Phase BLDC Motor Inverters Design

2.3.1. Y-Connection and Delta-Connection BLDC Motor Inverter Design

The inverter structure for both Y-Connection and Delta-Connection BLDC motors, as shown in Figure 4, is identical. It utilizes six switching components for driving the motor and comprises three half-bridge inverters. In the Y-Connection configuration, as depicted in Figure 4, junctions are formed by A-, B-, and C-. Additionally, A+, B+, and C+ are each connected to their respective half-bridge inverters. Conversely, for Delta-Connection, A+B-, B+C-, and C+A- form the junctions, connecting to the corresponding parts of the half-bridge inverter. The control sequence based on Hall Sensor signals, which is illustrated in Table 1, remains the same for both wiring configurations [19].

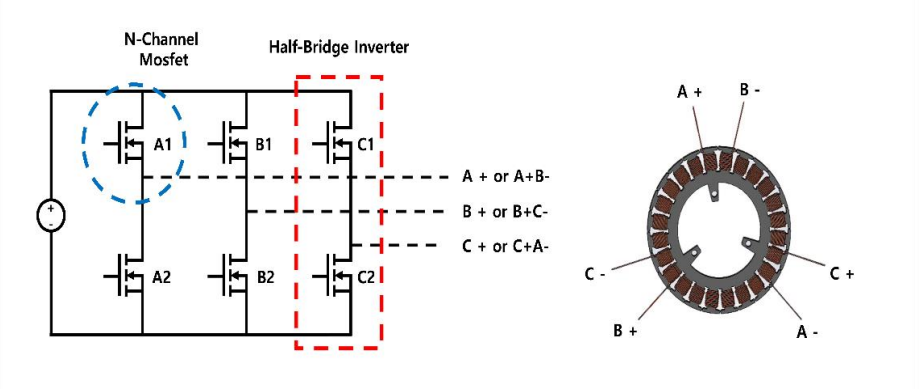

Figure 4. Y-Connection and Delta-Connection BLDC Motor Inverter Circuit and Connecting Schematic.

 doi:10.20944/preprints202403.1881.v1

Table 3. Y-Connection and Delta-Connection BLDC Motor Hall Sensor and Phase Sequence.

Direction	Operating Range		Hall Sensor			Switching Signal					
	Degree	Interrupt	HA	HB	HC	A1	A2	B1	B2	C1	C2
Forward	0~60	HA↑	1	0	1	1	0	0	PWM	0	0
	60~120	HC↓	1	0	0	1	0	0	0	0	PWM
	120~180	HB↑	1	1	0	0	0	1	0	0	PWM
	180~240	HA↓	0	1	0	0	PWM	1	0	0	0
	240~300	HC↑	0	1	1	0	PWM	0	0	1	0
	300~360	HB↓	0	0	1	0	0	0	PWM	1	0
Reverse	0~60	HA↑	1	1	0	0	0	0	PWM	1	0
	60~120	HB↓	1	0	0	0	PWM	0	0	1	0
	120~180	HC↑	1	0	1	0	PWM	1	0	0	0
	180~240	HA↓	0	0	1	0	0	1	0	0	PWM
	240~300	HB↑	0	1	1	1	0	0	0	0	PWM
	300~360	HC↓	0	1	0	1	0	0	PWM	0	0

2.3.2. Independent 3-Phase BLDC Motor Inverter Design

Unlike the six-step inverters of Y-Connection BLDC motors and Delta-Connection BLDC Motors, the inverter structure of the Independent 3-Phase BLDC Motor, as shown in Figure 5, consists of three full-bridge inverters, with each full-bridge inverter controlling the on/off of one phase. The connection between the stator and a single pole in the inverter is as illustrated in Figure 5. Furthermore, the Independent 3-Phase BLDC Motor has an identical electrical location with Y-Connection BLDC motors and Delta-Connection BLDC Motors. As a result, controlling the signals output based on the Hall Sensor signals is easily achievable using the same Hall Sensor signals as shown in Table 2 [20].

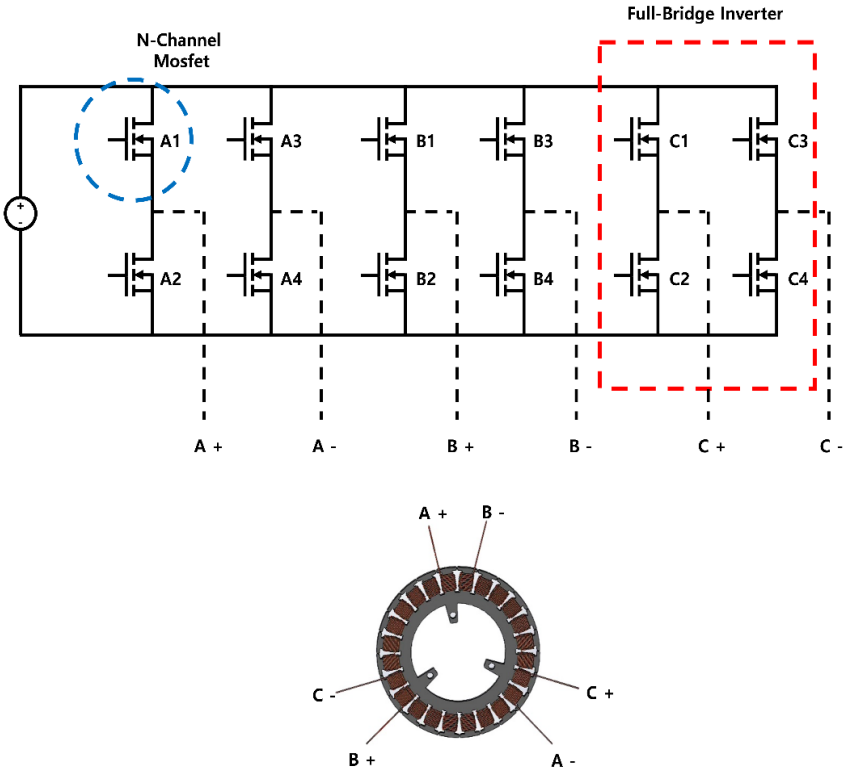

Figure 5. Independent 3-Phase BLDC Motor Inverter Circuit and Connecting Schematic.

 doi:10.20944/preprints202403.1881.v1

3. Experiment Comparing the Motor Dynamics

3.1. Experiment Design and Parameters

The proposed experiment's overall layout and experimental test bed are depicted in Figure 6 and Figure 7. The aim of the experiment is to compare the dynamic characteristics of Y-Connection BLDC Motors, Delta-Connection BLDC Motors, and Independent 3-Phase BLDC Motors to determine which winding structure is most suitable for robot joint actuators. To prevent variations in motor parameters due to changes in coil length based on the motor's wiring junctions, the junctions for Y-Connection and Delta-Connection were made within the motor driver's PCB. The parameters of the BLDC motors, including the stator resistance, the rated voltage is 24 V and the switching frequency is 18kHz. Speed calculation was performed using Hall sensor signals, and current measurement was performed using shunt resistors located at the bottom of the motor driver's inverter.

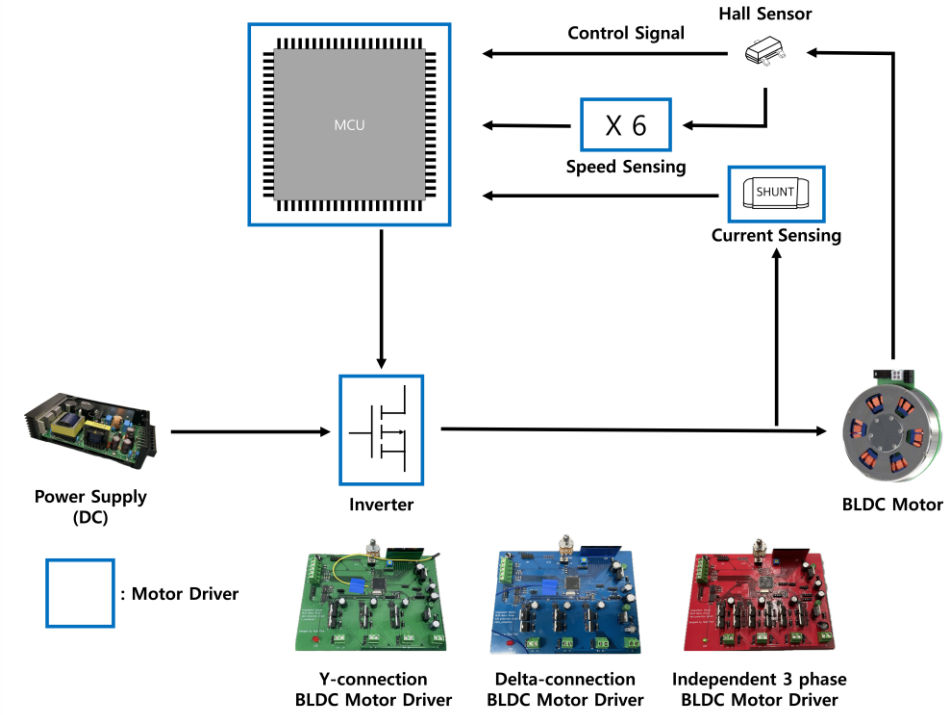

Figure 6. Experiment Setup Schematic.

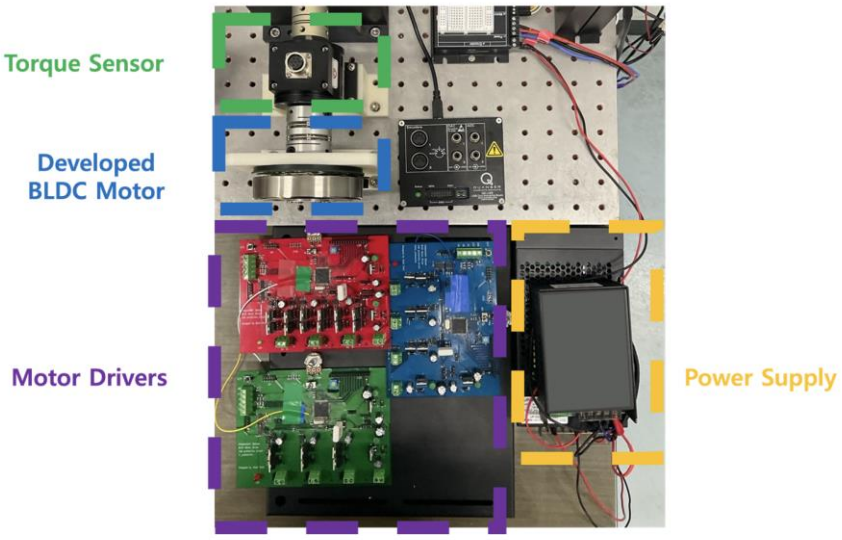

 doi:10.20944/preprints202403.1881.v1

Figure 7. Top View of the Experimental Test Bed.

3.2. Speed Experiment of Each BLDC Motor

The speed was calculated using the M method, using signals from the Hall sensors that were amplified sixfold to increase resolution. The equations for the M method are as provided in (4) and (5), and the parameters used for speed calculation are detailed in Table 4 [2]. The first comparative analysis of motor dynamics was conducted with PWM ranging from 30% to 90%, measuring the RPM changes corresponding to each duty ratio. In the second comparative analysis experiment, the characteristics of speed and current were compared at a 90% duty ratio.

$$\theta = \frac{m1}{PPR} \times 2\pi\ [rad] \tag{4}$$

$$\omega_m = \frac{60}{2\pi} \times \frac{\theta}{t} = \frac{60}{2\pi} \times \frac{m1}{PPR} \times 2\pi \times \frac{1}{T_s}\ [RPM] \tag{5}$$

Here, θ represents the rotation angle, poles indicate the number of poles in the motor, and PPR (Pulse Per Revolution) refers to the maximum number of output pulses per revolution of the motor. T_s represents the sampling time.

Table 4. Independent 3-Phase BLDC Motor Hall Sensor and Phase Sequence.

Direction	Operating Range		Hall Sensor			Switching Signal											
	Degree	Interrupt	HA	HB	HC	A1	A2	A3	A4	B1	B2	B3	B4	C1	C2	C3	C4
Forward	0~60	HA↑	1	0	1	1	0	0	PWM	0	PWM	1	0	0	0	0	0
	60~120	HC↓	1	0	0	1	0	0	PWM	0	0	0	0	0	PWM	1	0
	120~180	HB↑	1	1	0	0	0	0	0	1	0	0	PWM	0	PWM	1	0
	180~240	HA↓	0	1	0	0	PWM	1	0	1	0	0	PWM	0	0	0	0
	240~300	HC↑	0	1	1	0	PWM	1	0	0	0	0	0	1	0	0	PWM
	300~360	HB↓	0	0	1	0	0	0	0	0	PWM	1	0	1	0	0	PWM
Reverse	0~60	HA↑	1	1	0	0	0	0	0	0	PWM	1	0	1	0	0	PWM
	60~120	HB↓	1	0	0	0	PWM	1	0	0	0	0	0	1	0	0	PWM
	120~180	HC↑	1	0	1	0	PWM	1	0	1	0	0	PWM	0	0	0	0
	180~240	HA↓	0	0	1	0	0	0	0	1	0	0	PWM	0	PWM	1	0
	240~300	HB↑	0	1	1	1	0	0	PWM	0	0	0	0	0	PWM	1	0
	300~360	HC↓	0	1	0	1	0	0	PWM	0	PWM	1	0	0	0	0	0

Table 5. Speed Calculation Parameters for the M Method.

	Number of Poles	PPR	T_s(Sampling time) [sec]
BLDC motor	26	78	0.04

4. Results

In the first dynamic characteristic comparison experiment, the change in speed with respect to the change in duty ratio from 30% to 90% is shown in Figure 8. As shown in Section 2, in the case of the Independent 3-Phase BLDC Motor, which is a single-phase excitation system, since one voltage source can be used entirely by one phase, it can be seen that it achieves a higher speed at the same duty ratio. In the experiment, it was confirmed that noise and vibration, which did not occur in the Independent 3-Phase BLDC Motor and Y-Connection BLDC Motor, occurred in the Delta-Connection BLDC Motor. This can be attributed to the third harmonic present in the Delta-Connection and the imbalance of the voltage applied to each phase.

The second dynamic characteristic comparison experiment is shown in Figure 9, and the average speed and current were measured at 90% duty ratio. Figure 9 (a) shows the speed and current data

 doi:10.20944/preprints202403.1881.v1

of the Independent 3-Phase BLDC Motor, with an average speed of 700.1412 RPM and an average current value of 0.2707 A. The maximum current value was measured as 0.6780 A, confirming that a current ripple of approximately 0.4 A occurred at maximum. Figure 9 (b) shows the Y-Connection BLDC Motor, with an average speed of 368.1172 RPM and an average current value of 0.1218 A. The maximum current value was 0.3589 A, and the current ripple was confirmed to be approximately 0.2471 A. Comparing the data of these two winding structures, it can be confirmed that the Independent 3-Phase BLDC Motor, which is a single-phase excitation system, has an average speed value about twice as high as the Y-Connection BLDC Motor, which is a two-phase excitation system. As described in Section 2, this value is similar to the theory that the Independent 3-Phase BLDC Motor, which uses the full voltage in each phase, shows twice the speed compared to the Y-Connection BLDC Motor, which uses half of the total voltage in each phase. Figure 9 (c) shows the Delta-Connection BLDC Motor, with an average speed measured as 613.4125 RPM, and the average current value and maximum current value measured as 0.2430 A and 1.3588 A, respectively. Therefore, the maximum ripple is 1.1158 A. It can be confirmed that the average speed shows a saturation speed about √3 times higher compared to the Y-Connection BLDC Motor, as shown in the theory. It can also be observed that the current values flowing in each phase are different, and the higher ripple current measured can be attributed to the imbalance in the voltage across each phase and the presence of the third harmonic.

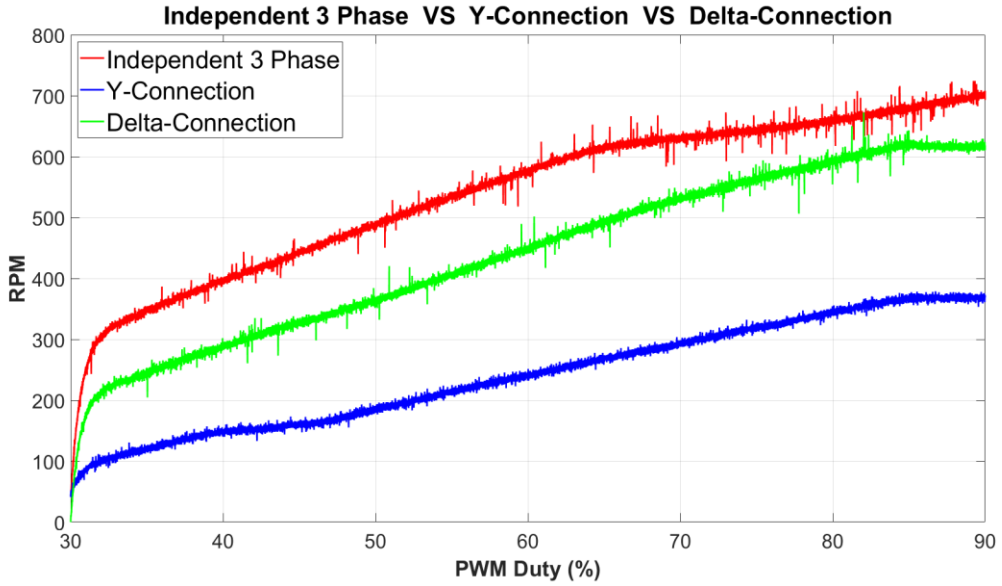

Figure 8. Comparison of Motor Speeds at PWM Duty 30~90%.

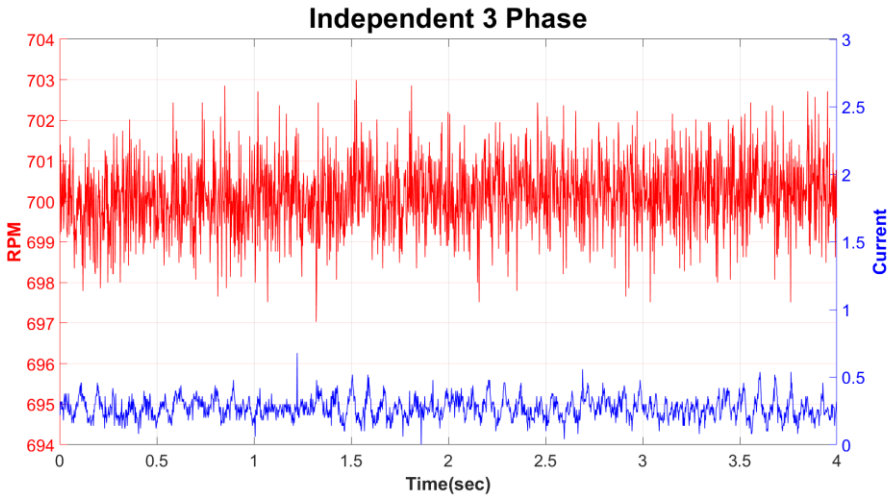

(a)

 doi:10.20944/preprints202403.1881.v1

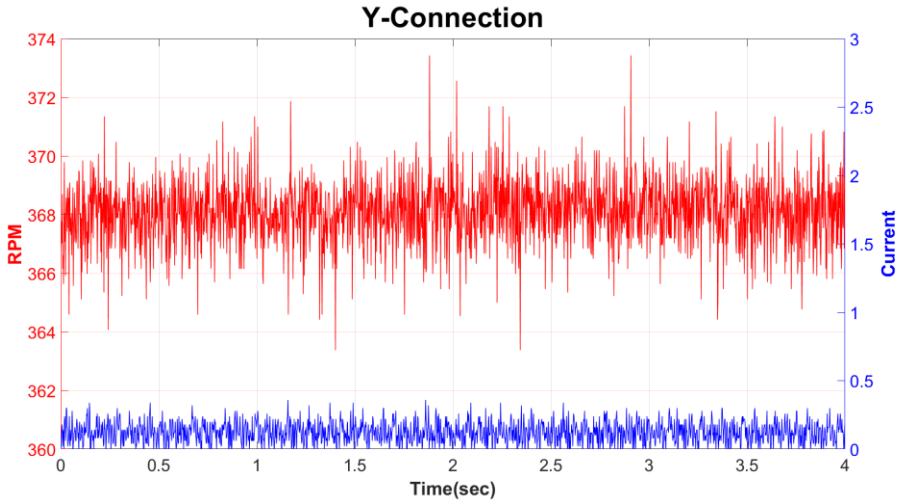

(b)

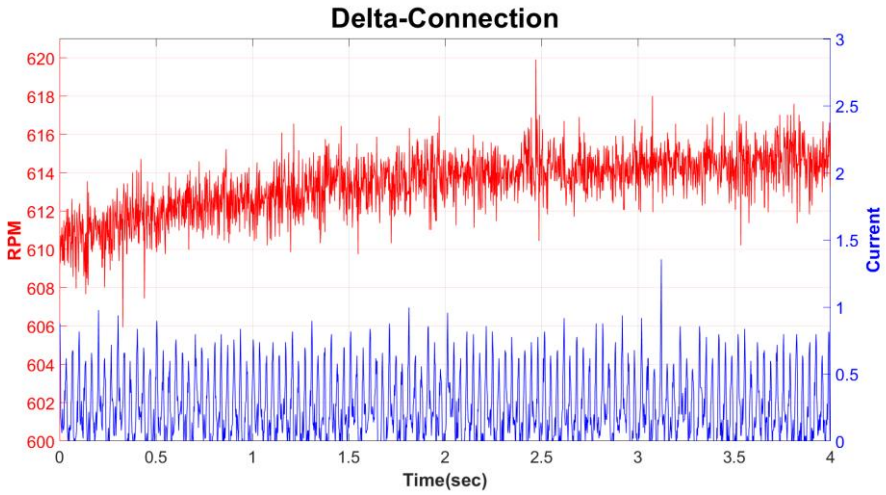

(c)

Figure 9. (a) Independent 3-Phase BLDC Motor RPM and Current at PWM Duty 90% (b) Y-Connection BLDC Motor RPM and Current at PWM Duty 90% (c) Delta-Connection BLDC Motor RPM and Current at PWM Duty 90%.

5. Discussion

Through a comparative analysis of motor characteristics, we sought to determine the most suitable wiring structure for BLDC motors in robot joint actuators. Our investigation compared the commonly used Y-Connection and Delta-Connection methods with the Independent 3-Phase BLDC Motor, which controls three distinct phases without junctions.

As shown in Figure 8, it was confirmed that the Independent 3-Phase BLDC Motor achieved the highest speed in all regions as the duty ratio increased from 30% to 90%. Additionally, as outlined in Table 5, in experiments comparing speed and current under identical voltage and duty ratios, the speed output exhibited the following trend: Independent 3-Phase BLDC Motor > Delta-Connection BLDC Motor > Y-Connection BLDC Motor. Moreover, comparing Independent 3-Phase BLDC Motor with Y-Connection BLDC Motor, the former exhibited approximately 1.9 times higher speed, even though with a value about 4.9% lower than the theoretical value. Similarly, in comparing Y-Connection BLDC Motor with Delta-Connection BLDC Motor, the latter showed a speed approximately 1.67 times higher, yet about 3.79% lower than the theoretical value of $\sqrt{3}$ times the speed saturation point. Additionally, comparing Independent 3-Phase BLDC Motor with Delta-Connection BLDC Motor, while theoretically both types of motors should have the same saturation speed, experimental results revealed that Independent 3-Phase BLDC Motor had about 86.73 RPM,

 doi:10.20944/preprints202403.1881.v1

1.14 higher speed. Therefore, these speed characteristic comparison results demonstrate that the speed characteristics of the motor can be improved by changing the winding structure of the motor.

Table 5. Mean RPM, Mean Current and Max Ripple Current at PWM Duty 90%.

	Independent 3-Phase	Y-Connection	Delta-Connection
RPM	700.1412	368.1172	613.4125
Current [A]	0.2707	0.1218	0.2430
Max Ripple [A]	0.6780	0.3589	1.3558

The average current values follow the sequence: Independent 3-Phase BLDC Motor > Delta-Connection BLDC Motor > Y-Connection BLDC Motor. However, there's a minimal difference in the average current values between the Independent 3-Phase BLDC Motor and the Delta-Connection BLDC Motor, with a variance of approximately 0.03 A. Furthermore, as depicted in Figure 9, the Delta-Connection BLDC Motor exhibits ripple currents five times larger than the average current, marking it as the motor with the highest current ripple among the three types. This can be attributed to the influence of the third harmonic in Delta-Connection BLDC Motors and the imbalance in voltage across phases. Motors generating significant ripple currents also tend to exhibit corresponding torque ripple, making them challenging for use in robotic joints. Therefore, upon examining the results, it becomes evident that the current characteristics of the Independent 3-Phase BLDC Motor are superior to those of the Delta-Connection BLDC Motor.

Through the above comparison of speed and current characteristics, it was shown that the Independent 3-Phase BLDC Motor can compensate for the disadvantages of high torque density motors. Consequently, this application can promote the use of high torque density motors in the actuators of robots that physically interact with humans. Furthermore, when high torque density motors are applied to robot joints, the lower gear dependency can lead to the reduction of nonlinear friction, enabling the estimation of torque from motor current and eliminating the need for torque sensors. Moreover, wearable robots, walking robots, and other robots that require batteries should have excellent characteristics at low voltages due to the size and weight limitations of battery packs. In this regard, the Independent 3-Phase BLDC Motor has an additional advantage, as it exhibits the best dynamic characteristics at the same voltage compared to other motor types. These contributions lead to a reduction in joint volume and weight, as well as a decrease in manufacturing costs, and this virtuous cycle greatly contributes to the advancement of robots.

However, there are several drawbacks to using an Independent 3-Phase BLDC Motor. Firstly, it may not be widely available on the market compared to Y-Connection and Delta-Connection BLDC Motors, along with the difficulty in obtaining Independent 3-Phase BLDC Motor drivers. Secondly, while the increase in torque density allows for the achievement of desired torque with lower current consumption, the need of twice as many switching components in the inverter compared to conventional Six-Step Inverters leads to a doubling of switching losses. Although losses due to switching components increase linearly, losses due to Joule heating increase quadratically with current, making it advantageous to minimize losses caused by Joule heating. Despite these drawbacks, increasing motor torque density remains essential for addressing the fundamental challenges in the development of robots that physically interact with humans. It is anticipated to contribute significantly to overcoming existing stagnation in the robotics industry and advancing human-robot interaction capabilities.

In the future work, to achieve significantly higher torque density and high speed within the robotic actuators themselves, we will develop multi-phase independent motors and motor drivers based on the Independent 3-Phase BLDC Motor. Afterward, we will apply these advancements to robotic joints and secure back-drivability to enhance both performance and safety in physical human-robot interaction. These advancements will contribute to the research field of safe physical interaction between humans and robots.

Author Contributions: Conceptualization, J.P. and H.C.; methodology, J.P. and H.C.; software, J.P.; data curation, J.P. and H.C.; formal analysis, J.P. and H.C.; writing-original draft preparation, J.P.; writing-review and editing, J.P. and H.C.; supervision, H.C.; project administration, H.C.; funding acquisition, H.C. All authors have read and agreed to the published version of the manuscript.

Funding: This work was supported by Incheon National University (International Cooperative) Research Grant in 2019.

Data Availability Statement: Data are contained within the article.

Conflicts of Interest: The authors declare no conflict of interest.

References

1. Pervez, A.; Ryu, J. Safe physical human robot interaction-past, present and future. J. Mech. Sci. Technol. 2008, 22, 469-483.
2. Suzumori, K.; Faudzi, A.A. Trends in hydraulic actuators and components in legged and tough robots: a review. Adv. Robot. 2018, 32, 458-476.
3. Ali, H.I.; Noor, S.B.B.M.; Bashi, S.M.; Marhaban, M.H. A review of pneumatic actuators (modeling and control). Aust. J. Basic Appl. Sci. 2009, 3, 440-454.
4. Seok, S.; Wang, A.; Otten, D.; Kim, S. Actuator design for high force proprioceptive control in fast legged locomotion. In Proceedings of the 2012 IEEE/RSJ International Conference on Intelligent Robots and Systems, Vilamoura, Portugal, 7-12 October 2012; pp. 1970-1975.
5. Seok, S.; Wang, A.; Chuah, M.Y.M.; Otten, D.; Lang, J.; Kim, S. Design principles for highly efficient quadrupeds and implementation on the MIT Cheetah robot. In Proceedings of the 2013 IEEE International Conference on Robotics and Automation, Karlsruhe, Germany, 6-10 May 2013; pp. 3307-3312.
6. Seok, S.; Wang, A.; Chuah, M.Y.; Hyun, D.J.; Lee, J.; Otten, D.M.; Lang, J.H.; Kim, S. Design principles for energy-efficient legged locomotion and implementation on the MIT cheetah robot. IEEE/ASME Trans. Mechatron. 2014, 20, 1117-1129. Seok,
7. Wensing, P.M.; Wang, A.; Seok, S.; Otten, D.; Lang, J.; Kim, S. Proprioceptive actuator design in the MIT cheetah: Impact mitigation and high-bandwidth physical interaction for dynamic legged robots. IEEE Trans. Robot. 2017, 33, 509-522..
8. Farve, N.N. Design of a low-mass high-torque brushless motor for application in quadruped robotics. Ph.D. Thesis, Massachusetts Institute of Technology, Cambridge, MA, USA, 2012.
9. Jo, K.-J.; Oh, J.-S. Characteristic analysis of independent 3 phase BLDC motor. Trans. Korean Inst. Power Electron. 2007, 12, 299-304.
10. Farve, N.N. Design of a low-mass high-torque brushless motor for application in quadruped robotics. Ph.D. Thesis, Massachusetts Institute of Technology, Cambridge, MA, USA, 2012.
11. Yu, S.; Wang, Z.; Gan, H.; Shi, Q.; Wang, Z.; Xiao, Y.; Zhang, J.; Zhao, J. Quasi-direct drive actuation for a lightweight hip exoskeleton with high backdrivability and high bandwidth. IEEE/ASME Trans. Mechatron. 2020, 25, 1794-1802.
12. Mohanraj, D.; Muthananthguruadoss, S.; Vijayarajan, A.; Rajasekar, V.G.; Chokkalingam, B.; Muthuramalingam, T. A review of BLDC motor: state of art, advanced control techniques, and applications. IEEE Access 2022, 10, 54833-54869.
13. Park, D.-H.; Chun, Y.-H.; Lee, K.-H.; Koo, B.-K. Current Compensation Scheme to Reduce Torque Ripples of Delta-connected Low-inductance BLDC Motor Drives. Trans. Korean Inst. Power Electron. 2017, 22, 449-456.
14. Pillay, P.; Krishnan, R. Modeling of permanent magnet motor drives. IEEE Trans. Ind. Electron. 1988, 35, 537-541.
15. Pillay, P.; Krishnan, R. Modeling, simulation, and analysis of permanent-magnet motor drives. II. The brushless DC motor drive. IEEE Trans. Ind. Appl. 1989, 25, 274-279.
16. Kim, Y.; Yoon, Y.-D.; Sul, S.-K. Design and control methodology analysis of BLDC motor for torque ripple minimization considering winding connection. In Proceedings of the 2013 International Conference on Electrical Machines and Systems (ICEMS), Busan, South Korea, 26-29 October 2013; pp. 1138-1141.
17. Heo, C.-N.; Hwang, S.-H. Air-gap Control According to Y and Delta Connections of Double-sided Air-gap Permanent Magnet Synchronous Motor with Independent Three-phase Structure. Trans. Korean Inst. Power Electron. 2017, 22, 249-255.
18. Lee, T.-Y.; Chun, Y.-H.; Ahn, J.-M.; Lee, J.; Chun, T.-W. Design and torque ripple analysis of brush-less dc motor according to delta winding connection. J. Magn. 2015, 20, 166-175.
19. Lee, Y.; Kim, J. Analysis of the three-phase inverter power efficiency of a BLDC motor drive using conventional six-step and inverted pulsewidth modulation driving schemes. Can. J. Electr. Comput. Eng. 2019, 42, 34-40.

 doi:10.20944/preprints202403.1881.v1

20. Sun, Q.; Wu, J.; Gan, C.; Si, J.; Guo, Y. Modular full-bridge converter for three-phase switched reluctance motors with integrated fault-tolerance capability. IEEE Trans. Power Electron. 2018, 34, 2622-2634.
21. Petrella, R.; Tursini, M.; Peretti, L.; Zigliotto, M. Speed measurement algorithms for low-resolution incremental encoder equipped drives: a comparative analysis. In Proceedings of the 2007 International Aegean Conference on Electrical Machines and Power Electronics, Bodrum, Turkey, 10-12 September 2007; pp. 780-787.